Journal of Power Sources 194 (2009) 190–198

Contents lists available at ScienceDirect

Journal of Power Sources

journal homepage: www.elsevier.com/locate/jpowsour

A droplet size dependent multiphase mixture model for two phase flow in PEMFCs

Guangli He [a], Yohtaro Yamazaki [a,*], Abuliti Abudula [b]

[a] Department of Innovative and Engineered Materials, Interdisciplinary Graduate School of Science and Engineering, Tokyo Institute of Technology, Tokyo, Japan
[b] New Energy Technology Research Division, Aomori Industrial Research Center, Aomori, Japan

ARTICLE INFO

Article history:
Received 16 January 2009
Received in revised form 24 March 2009
Accepted 11 May 2009
Available online 20 May 2009

Keywords:
Droplet
Multiphase mixture model
Two phase flow
PEMFC
Fuel cell

ABSTRACT

A droplet size dependent multiphase mixture model is developed in this paper, and the droplet size in the gas channel can be considered as a parameter in this multiphase mixture model, which includes the effect of gas diffusion layer (GDL) properties and the gas drag function and cannot be considered in the commonly used multiphase mixture model in the references. The three-dimensional two phase and non-isothermal simulation of the PEMFCs with a straight flow field is performed. The effect of droplet size on the liquid remove, the effect of liquid water on the heat transfer and the effect of gas flow pattern on the heat and mass transfer are mainly investigated. The simulation results show that the large droplet is hard to be dragged by the gas, so it produces large water saturation. The results of the heat transfer show that the liquid water hinders the heat transfer in the GDL and catalyst layer, so it produces the large relative high temperature area, and there are large temperature difference and water saturation in the PEMFCs operated with coflow pattern compared with counter flow pattern.

1. Introduction

Water management is very important for the operation of PEMFCs. Keeping the membrane with enough water content and removing the excessive liquid water effectively are the main focus of water management, which directly affect performance and heat management of the PEMFCs. Liquid water transport in PEMFCs occurs as follows: (1) water is produced in cathode catalyst layer, and liquid water transports within the gas diffusion layer (GDL) by capillary-driven flow. (2) Liquid water droplets appear on the GDL/gas channel interface and are removed by the gas shearing function [1–4]. (3) Liquid water travels in the gas channel. Wang and his coworkers [3] have observed the emergence, growth and detachment of liquid water droplet on the GDL/gas channel interface. And they [5] have measured the size of the droplet on the GDL/gas channel interface, and find that liquid water can transport through the gas channel without interaction with channel wall at high gas velocity. Also, Kimball et al. [6,7] have proved that the liquid water flow through the largest pore of the hydrophobic gas diffusion layer, in their experiments, it was found that the liquid water appeared at the same position for the different operating condition, which shows the new way for the analysis and insight knowing of the liquid transportation in the gas diffusion layer.

By now, many models have been developed for simulating the liquid water transport in PEMFCs. Those models are based on the different theory and assumption in flow dynamics. One of the most commonly used model is the multiphase mixture (M^2) model, which consider the liquid and the gas as mixture [8–13] simply and calculation cost effectively. However, two phase flows in PEMFCs are complex dynamic processes. Gurau et al. [13] show that the M^2 model has a narrow range of applicability, which is limited to steady-state flows without change of phase and without phase production due to other physical processes. For more complex situations, including those commonly encountered in PEMFCs, the M^2 model ceases to reflect the principles and could lead to predictions of unrealistic velocity and scalar fields. Furthermore, the M^2 model could represent a tool unable to capture complex fuel cell phenomena such as water transfer and the liquid droplet in the gas channel and its effect on the mass transfer cannot be considered in the multiphase mixture model. In the recent works, the two-fluid model has obtained more attention for its convenience of considering the liquid phase and gas phase separately, so it can describe more phenomena in the two phase flow [14–16], but there are also some disadvantages for the two-fluid model, such as it needs more calculation cost, and its hard to converge for it includes the liquid momentum equation, liquid continuity equation, gas momentum equation, and gas continuity equation.

In this paper, we developed a droplet size dependent multiphase mixture model for considering the two phase behavior in PEMFCs. In this model, the interacting effect between two phases is

* Corresponding author. Tel.: +81 45 924 5411; fax: +81 45 924 5411.
E-mail address: yamazaki.y.af@m.titech.ac.jp (Y. Yamazaki).

0378-7753/$ – see front matter © 2009 Elsevier B.V. All rights reserved.
doi:10.1016/j.jpowsour.2009.05.008

Nomenclature

Parameters and variables

a	acceleration
C_D	drag coefficient
c_T	mass transfer coefficient
D	diffusion coefficient ($cm^2\ s^{-1}$)
d_p	characteristic droplet size (cm)
F	Faraday's constant
f_{drag}	drag function
M	molar mass ($kg\ mol^{-1}$)
M_l	interface force of liquid (N)
M_g	interface force of gas (N)
n	number of electrons
P	pressure (Pa)
q	switch function
R	universal gas constant ($J\ mol^{-1}\ K^{-1}$)
R_{cat}	reaction rate in cathode
R_{an}	reaction rate in anode
Re	Reynold number
s	water saturation
T	temperature (K)
V	velocity ($cm\ s^{-1}$)
V_{oc}	open circuit voltage (V)
y	molar fraction

Greek letters

ϕ	potential (V)
ε	volume fraction
σ	surface tension ($N\ cm^{-1}$)
θ_c	equilibrium contact angle on diffuser
λ	polymer water content H_2O/SO_3
α_d	drag coefficient of water in membrane
η	overpotential (V)
μ	viscosity (Pa s)
ρ	density ($kg\ cm^{-3}$)
τ_p	relaxation time

Subscripts

an	anode
C	about capillary
cat	cathode
dr	drift
sat	saturated
sol	about electron
g	gas phase
H_2	hydrogen
i	note for species
k	note for phases
l	liquid phase
m	mixture properties of multiphase mixture
mem	polymer phase
O_2	oxygen
p	phase
q	pahse
R	relative
w	water
wv	water vapor

considered in a multiphase mixture form, which includes the effect of the droplet size, the drag coefficient, velocity, Reynolds number, the droplet relaxation time. Compared with the two-fluid model, the present model is calculation cost effective and it is easy to be performed, also it can includes the effect of the droplet size on the liquid removal compared with the mixture model, which is a key factor in two phase flow in PEMFCs. However, the gas channel wall contact angle can affect the liquid form in the gas channel, and the hydrophobic gas channel wall likely produces droplet, but hydrophilic channel wall likely produces water film. The interaction between gas and the liquid film is more complex than that of water droplet, that is will be considered in the future work. So, the present model is preferable for PEMFCS with hydrophobic gas channel.

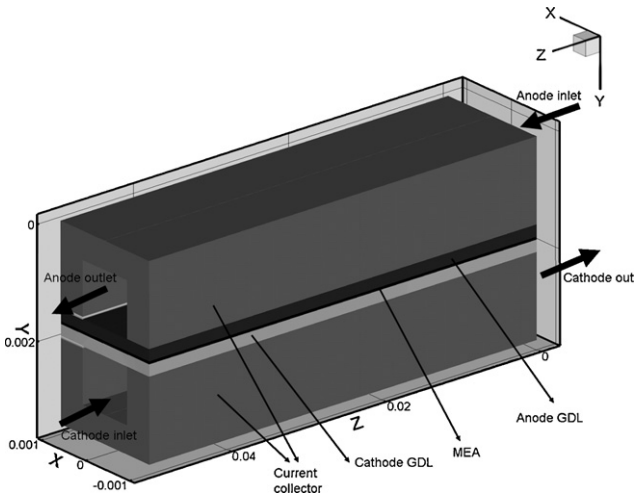

Fig. 1. Geometry model for the simulation.

2. Model development

2.1. Model assumption

The calculated regions consist of conventional straight channels, gas diffusion electrodes, catalyst layers and a membrane, as well as current collectors, which are shown in Fig. 1. Because PEMFC is operated in temperature of 80 °C, so it is assumed that water is generated in cathode catalyst layer as liquid, and the mss transfer between liquid phase and gas phase are considered. Because it is a steady state model in this work, so the growing up process for the droplet cannot be considered, and also, the effect of gas channel wall is not involved in this model. In the gas diffusion layer and catalyst layer, the liquid driven force is capillary force, which is the function of water saturation, so the other forces are not considered.

2.2. Governing equations

The droplet size dependent multiphase mixture model is developed as follows:

The continuity equation for the multiphase mixture is

$$\frac{\partial}{\partial t}(\rho_m) + \nabla \cdot (\rho_m \vec{v}_m) = 0 \tag{1}$$

$$\vec{v}_m = \frac{\sum_{k=1}^{n} \alpha_k \rho_k \vec{v}_k}{\rho_m} \tag{2}$$

$$\rho_m = \sum_{k=1}^{n} \alpha_k \rho_k \tag{3}$$

The momentum equation for the mixture can be expressed as:

$$\frac{\partial}{\partial t}(\rho_m \vec{v}_m) + \nabla \cdot (\rho_m \vec{v}_m \vec{v}_m) = -\nabla p + \nabla \cdot [\mu_m (\nabla \vec{v}_m + \nabla \vec{v}_m^T)] + \rho_m \vec{g} + \vec{F} + \nabla \cdot \left(\sum_{k=1}^{n} \alpha_k \rho_k \vec{v}_{dr,k} \vec{v}_{dr,k} \right) \tag{4}$$

$$\mu_m = \sum_{k=1}^{n} \alpha_k \mu_k \tag{5}$$

$\vec{v}_{dr,k}$ is the drift velocity for secondary phase k:

$$\vec{v}_{dr,k} = \vec{v}_k - \vec{v}_m \tag{6}$$

The relative velocity is

$$\vec{v}_{pq} = \vec{v}_p - \vec{v}_q \tag{7}$$

The mass fraction for any phase (k) is defined as:

$$c_k = \frac{\alpha_k \rho_k}{\rho_m} \tag{8}$$

The drift velocity and the relative velocity ($\vec{v}_{qp}$) are connected by the following expression:

$$\vec{v}_{dr,p} = \vec{v}_{pq} - \sum_{k=1}^{n} c_k \vec{v}_{qk} \tag{9}$$

$$\vec{v}_{pq} = \frac{\tau_p}{f_{drag}} \frac{(\rho_p - \rho_m)}{\rho_p} \vec{a} \tag{10}$$

where τ_p is the particle relaxation time [17].

Particle relaxation time in two phase flow means the time in which the droplet's velocity change from zero to the equilibrium velocity with the gas phase. And

$$\tau_p = \frac{\rho_p d_p^2}{18 \mu_q} \tag{11}$$

The default drag function f_{drag} is taken from Schiller and Neumann [18]:

$$\begin{aligned}
&Re \le 0.01 && C_D = \frac{9}{2} + \frac{24}{Re} \\
&0.01 < Re < 20 && C_D = \frac{24}{Re}[1 + 0.1315 Re^{(0.82 - 0.05w)}] \\
&20 \le Re \le 260 && C_D = \frac{24}{Re}[1 + 0.1935 Re^{0.6305}] \\
&260 < Re \le 1.5 \times 10^3 && \log_{10} C_D = 1.6435 - 1.1242w + 0.1558w^2 \\
& && w = \log_{10} Re
\end{aligned} \tag{12}$$

and the acceleration $\vec{a}$ is of the form [19]:

$$\vec{a} = \vec{g} - (\vec{v}_m \cdot \nabla)\vec{v}_m - \frac{\partial \vec{v}_m}{\partial t} \tag{13}$$

From the continuity equation for phase p, the volume fraction equation for phase p can be obtained:

$$\frac{\partial}{\partial t}(\alpha_p \rho_p) + \nabla \cdot (\alpha_p \rho_p \vec{v}_m) = -\nabla \cdot (\alpha_p \rho_p \vec{v}_{dr,p}) + \sum_{q=1}^{n} (\dot{m}_{qp} - \dot{m}_{pq}) \tag{14}$$

In the gas difusion layer and catalyst layer, the liquid is driven by capillary force, then:

$$\frac{\partial(\varepsilon \rho_l s)}{\partial t} + \nabla \cdot \left[\rho_l \frac{K s^3}{\mu_l} \frac{dp_c}{ds} \nabla s \right] = r_w \tag{15}$$

And

$$p_c = \begin{cases} \frac{\sigma \cos\theta_c}{(K/\varepsilon)^{0.5}}(1.417(1-s) - 2.12(1-s)^2 + 1.263(1-s)^3) & \theta_c < 90^\circ \\ \frac{\sigma \cos\theta_c}{(K/\varepsilon)^{0.5}}(1.417s - 2.12s^2 + 1.263s^3) & \theta_c > 90^\circ \end{cases} \tag{16}$$

The mass transfer rate r_w between two phases is

$$c_r \max\left(\left[(1-s) \frac{P_{wv} - P_{sat}}{RT} M_{w,H_2O} \right], [-8\rho_l] \right) \tag{17}$$

The species mass conservation in phase p is

$$\nabla \cdot (\alpha_g \rho_g \overrightarrow{v}_g y_i) = \nabla \cdot (D_i \nabla y_i) + S_i \tag{18}$$

And, v_g can be obtained according to Eqs. (6), (7) and (10), source term for the gas phase is

$$S_{H_2} = -\frac{M_{w,H_2}}{2F} R_{an} \tag{19}$$

$$S_{O_2} = -\frac{M_{w,O_2}}{4F} R_{cat} \tag{20}$$

$$S_{H_2O} = \frac{M_{w,H_2O}}{2F} R_{cat} \tag{21}$$

In catalyst layer the relationship between species mass fraction on the catalyst surface and the reaction sites is

$$\frac{\rho D_i}{\delta}(y_{i,surf} - y_{i,cent})r = \frac{M_{w,i}}{nF} R_{an,cat} \tag{22}$$

The effective diffusion coefficient is [20]:

$$D_i = \varepsilon^{1.5}(1-s)^{r_s} D_i^0 \left(\frac{p_0}{p} \right)^{\gamma_p} \left(\frac{T}{T_0} \right)^{\gamma_t} \tag{23}$$

The membrane phase and solid phase potential conservation equations and electrochemical reaction rate in the cathode side and anode side:

$$\nabla \cdot (\sigma_{sol} \nabla \phi_{sol}) + R_{sol} = 0 \tag{24}$$

$$\nabla \cdot (\sigma_{mem} \nabla \phi_{mem}) + R_{mem} = 0 \tag{25}$$

$$R_{an} = j_{an}^{ref} \left(\frac{[H_2]}{[H_2]_{ref}} \right)^{\gamma_{an}} (e^{\alpha_{an} F \eta_{an}/RT} - e^{-\alpha_{cat} F \eta_{an}/RT}) \tag{26}$$

$$R_{cat} = j_{cat}^{ref} \left(\frac{[O_2]}{[O_2]_{ref}} \right)^{\gamma_{cat}} (-e^{+\alpha_{an} F \eta_{cat}/RT} - e^{-\alpha_{cat} F \eta_{cat}/RT}) \tag{27}$$

where

$$\eta_{an} = \phi_{sol} - \phi_{mem} \tag{28}$$

$$\eta_{cat} = \phi_{sol} - \phi_{mem} - V_{oc} \tag{29}$$

For the consideration of the effect of liquid, the reaction rate calculated in Eqs. (26) and (27) are multiplied by $(1 - s_l)$.

Membrane phase electric conductivity [21]:

$$\sigma_{mem} = \beta \varepsilon (0.514\lambda - 0.326)^w e^{1268((1/303) - 1/T)} \tag{30}$$

$$\alpha_d = 2.5 \frac{\lambda}{22} \tag{31}$$

$$\lambda = 0.043 + 17.18a - 39.85a^2 + 36a^3 (a < 1)$$

$$\lambda = 14 + 1.4(a-1) (a > 1) \tag{32}$$

$$a = \frac{P_{wv}}{P_{sat}} 2s \tag{33}$$

$$P_{wv} = x_{H_2O} P \tag{34}$$

$$\log_{10} P_{sat} = -2.1794 + 0.02953(T - 273.17) - 9.1837 \times 10^{-5}(T - 273.17)^2 + 1.4454 \times 10^{-7}(T - 273.17)^3 \tag{35}$$

Water diffusion flux through the membrane is

$$J_w^{diff} = -\frac{\rho_m}{M_m} M_{h20} D_l \nabla \lambda \tag{36}$$

And [21]

$$D_l = f(\lambda)e^{2416((1/303)-1/T)} \tag{37}$$

The heat conservation equation is

$$\nabla\cdot(\rho_m c_{pm}\vec{v_m}T) = \nabla\cdot(k_{eff}\nabla T) + S_h$$
$$T = \sum_{i=1}^{i=n}\frac{\alpha_i\rho_i T_i}{\rho_m}$$
$$k_{eff} = \varepsilon\sum_{i=1}^{i=n}\alpha_i k_i + (1-\varepsilon)k_s \tag{38}$$
$$c_{pm} = \sum_{i=1}^{i=n}\alpha_i c_{p,i}$$

S_h is calculated as follows:

$$S_h = I^2 R_{\text{ohm}} + h_{\text{reaction}} + \eta R_{\text{an,cat}} + h_{\text{phase}} \tag{39}$$

2.3. Boundary conditions and parameters

The inlet volume flow rate is 150 $cm^3\ min^{-1}$, which is converted to mass flow rate by the UDF (user defined function in Fluent® software), the outlet boundary condition is the pressure outlet condition, the outlet pressure is equal to atmosphere pressure. The inlet temperature is 353 K, and the temperature of anode current collector and cathode current collector end walls boundary are the 353 K, which means the current collector is ideally cooled. The other lateral walls and the end walls are impermeable for all the species. The operated potential is set on the boundary of cathode current collector. While the potential on the anode current collector boundary is set to be 0. The water saturation in cathode and anode inlet is zero. In the two-fluid model and the droplet size dependent multiphase mixture model in the present study, the droplet size in the gas channel is the key variable. Which integrate the effect of the properties of GDL and gas flow properties on the formation of liquid droplet, including the commonly used contact angle, and the pore size characters of the GDL, as well as the structure of GDL. There are some works which have concentrated on the determination of the droplet detachment diameter by the computational fluid dynamics (CFD) method [22–24] and analytical method [14], but the GDL structure cannot be considered in all those models, which is essential for water flow through the GDL to the gas channel [6,7]. So, the experiential formula for estimating the droplet size is applied as follows, which was completed by Wang and co-worker [5] for the certain experimental condition:

$$\log(d_p) = -2.59\log(v) + K - 1.59\log(1 + 5.2Re^{-0.63}) \tag{40}$$

The values of the other parameters used in the model are listed in Table 1.

2.4. Mesh grid and solution technique

The geometry model is shown in Fig. 1 and it is discretized into 550,500 hexahedral mesh volumes, and to assure the quality of the grid, the size of the grid in gas channel, gas diffusion layer, catalyst layer and membrane are different. The Simplec algorithm and Quick difference scheme are applied for solving the pressure–velocity coupled equations, and species equations. And suitable relax factors are used for momentum, slip velocity, water saturation, potential and species. The simulation is performed in Flunet® software of Ansys company with some codes of UDF (User Defined Function in Fluent) added by us.

Table 1
Values of the parameters.

Physical properties	Value
Faraday's constant, F	96487 C mol^{-1}
Permeability of gas diffusion layer, K_p	8×10^{-8} cm^2
Liquid water viscosity, μ_l	3.565×10^{-4} Pa s
Anodic transfer coefficient, α_a	0.5
Cathodic transfer coefficient, α_c	0.55
Water contact angle in diffuser, θ	120°
Gas channel width	0.1 cm
Gas channel length	5 cm
Gas channel height	0.1 cm
Thickness of current collector	0.15 cm
Anode GDL thickness	0.019 cm
Cathode GDL thickness	0.019 cm
Gas diffusion layer void fraction	0.7
Catalyst layer thickness	0.002 cm
Catalyst layer void fraction	0.5
Membrane thickness (Nafion® 112)	0.0005 cm
Cell inlet temperature	353 K
Outlet pressure	0.1 MPa
Air and fuel inlet humidified temperature	348 K
Open circuit voltage	0.95 V
Mass transfer rate between phases, c_T	200 s^{-1}
Gas constant, R	8314 J mol^{-1} K^{-1}
Reference hydrogen concentration, H_2^{ref} 1 kmol m^{-3}	
Reference oxygen concentration, O_2^{ref}	1 kmol m^{-3}
Operation current density	1.0 A cm^{-2}
Anode exchange current density, $j_{\text{an}}^{\text{ref}}$	1.5e8 A m^{-3}
Cathode exchange current density, $j_{\text{ca}}^{\text{ref}}$	7000 A m^{-3}
Thermal conductivity of GDL, membrane and CL, k	8 w m^{-1} k^{-1}
Thermal current collector	8 w m^{-1} k^{-1}
Specific heat capacity of liquid water	4182 J kg^{-1} k^{-1}
Electrical conductivity of GDL and CL	5000 1 ohm^{-1} m^{-1}

3. Results and discussion

3.1. Validity of the present work

In many references, the model of PEMFCs were validated by the comparison between the calculated performance and the experiment data, although it is impossible to account for all the factors for the performance in the model, there are still no more suitable method for validating the model results. In some references, the liquid water distribution was observed by optical method or neutron tomogram, but it is just the qualitative method. So, to explore the simple and precise model validated method is also a subject which should be paid more attention in the future work. To show the reasonability of the present model, the experimental data and

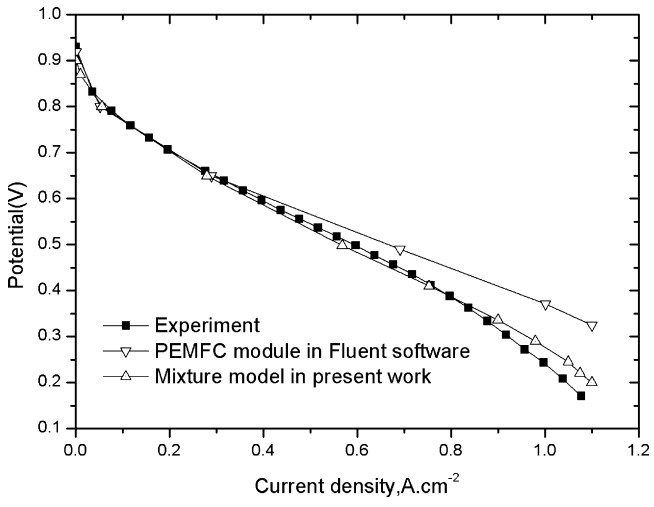

Fig. 2. Comparison between the experimental data and simulation result.

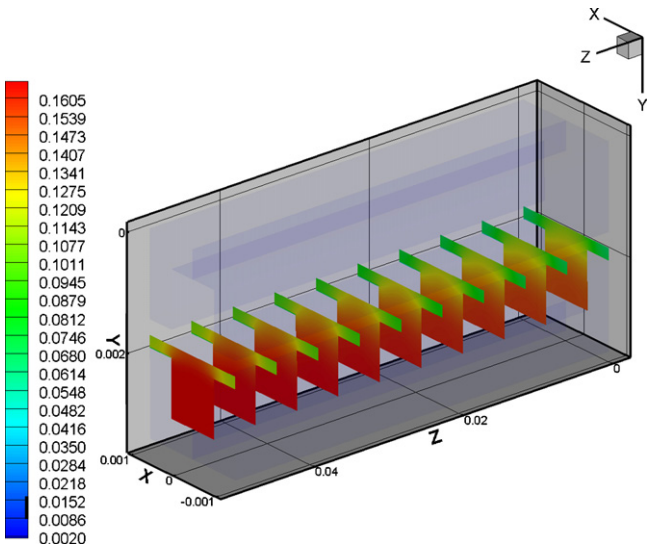

Fig. 3. Oxygen mass fraction in the cathode side for the base case.

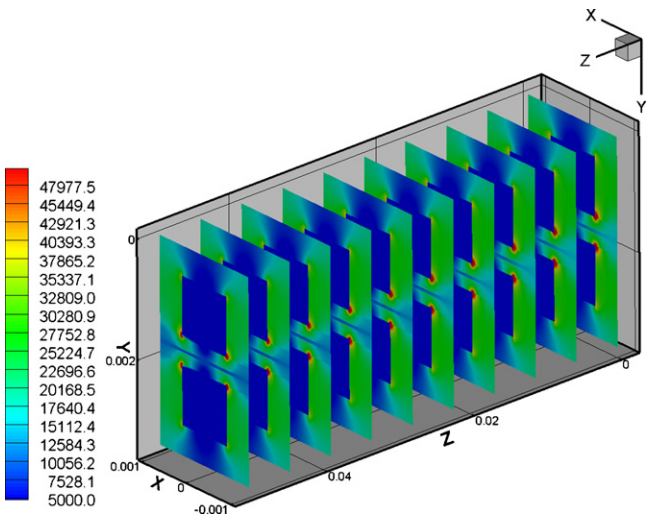

Fig. 5. Current density distribution in the PEMFCs for the base case, A m^{-2}.

the calculated result from PEMFCs Module (one of the add-in module) in Fluent® software are both used. Fig. 2 shows the comparison among the three results. It can be seen that the present model is more suitable than the PEMFCs Module for the high current density. Because the liquid is assumed to have the same velocity and only gas momentum equation is solved in the PEMFCs Module in Fluent software.

3.2. Species mass fraction, water saturation, and current density in the PEMFCs

Figs. 3–5 show the oxygen mass fraction, water saturation and current density distribution in the PEMFCs, respectively. As expected, the oxygen mass fraction decreases from inlet to outlet, from gas channel to catalyst layer. And the low oxygen mass fraction area appears in the catalyst layer and GDL neighboring to the rib of the current collector, where the longest distance exists for the gas convection and diffusion.

The same distribution characters are obtained for the water saturation shown in Fig. 4. However, liquid water behavior in the gas flow channels and GDL are very complicated, especially for the droplets in the gas flow channels, when the size of the droplet reaches a certain value, it may interact with the gas channel walls [25,5], then the liquid droplet maybe deform to liquid film if the channel wall is hydrophilic. Which are difficult to be considered in the mixture model or two-fluid model. And the results obtained in the two-fluid model or the mixture model for the water saturation are the volume-averaged values. So, the water saturation obtained in the GDL is more meaningful than that in the gas channel. And it can be observed in Fig. 4 that the current collector ribs hinder the liquid water removal so the water saturation in the GDL and catalyst layer neighboring to the ribs is higher compared with that neighboring the gas channel.

Fig. 5 shows the current density distribution in the whole PEMFCs, it can be seen that the highest current density appears in the corner between the gas channel and current collector ribs. Due to the current cannot be conducted through the channel so the current density is low in the area neighboring the gas channel top and bottom.

3.3. Effect of water saturation on the temperature distribution

Fig. 6 shows the temperature distribution in the PEMFCs for the base case (the operation current density is about 1.0 A cm^{-2}).

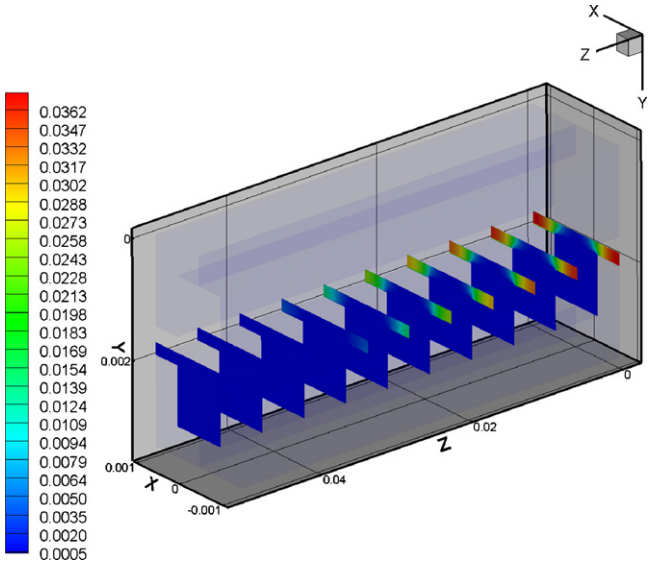

Fig. 4. Water saturation in the cathode side for the base case.

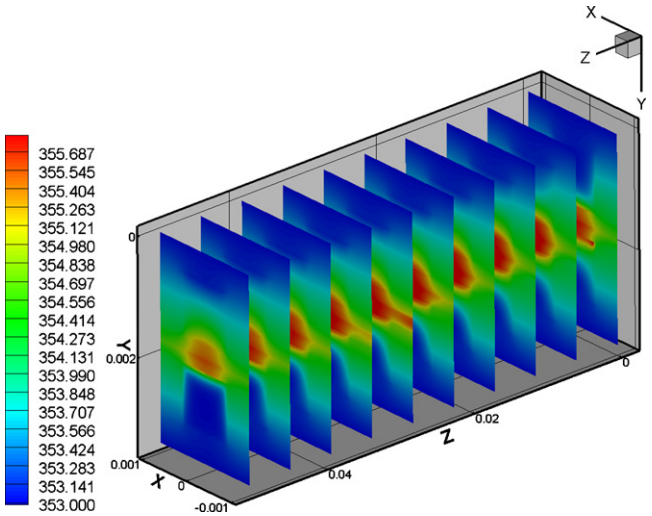

Fig. 6. The temperature distribution in the PEMFCs for the base case, *k*.

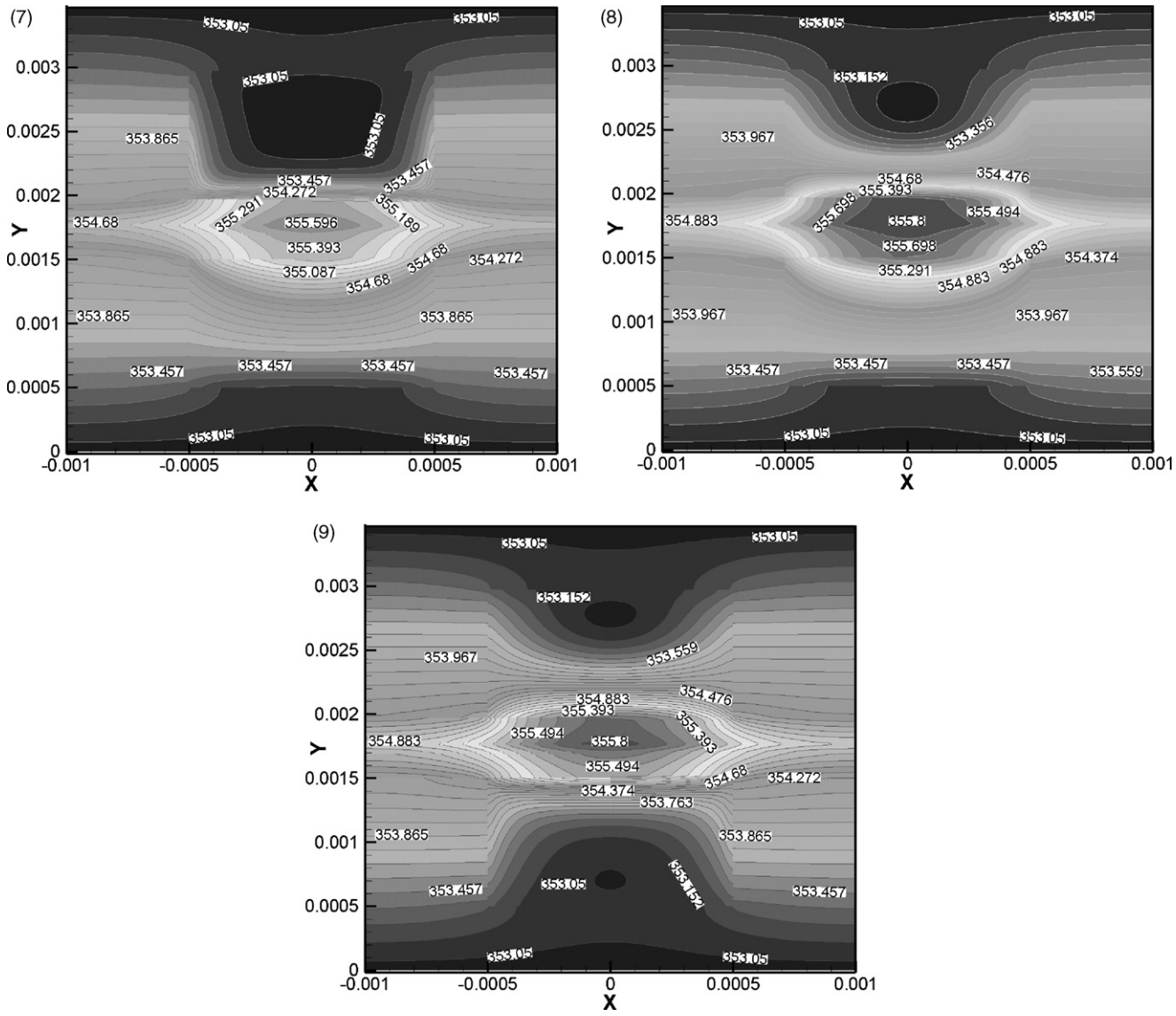

Fig. 7-Fig. 9. Temperature for the cross-section of $Z = 0.05$ m, $Z = 0.025$ m, $Z = 0$ m for the single phase case, *k*.

The lowest temperature could be observed at the flow inlet where the flows with constant temperature (353 K) come in, and the temperature increases slightly along the positive flow direction in the cathode channel and anode gas channel, but the temperature changes in anode channel is more obvious than that in cathode channel, this is due to the difference of thermal conductivity between air and hydrogen (the values of thermal conductivity for air and hydrogen are 0.0242 and 0.16 respectively). The heat generation is due to the electrochemical reaction and Ohmic heating. Therefore, the highest temperature concentrates in the catalyst layers in which the reactions take place and the current is generated. Especially in the area neighboring to the gas channel, the temperature is relative high for the weakness of the gas thermal conductivity. Due to the constant temperature for the coolant boundary, the change of temperature distribution through the current collector from inlet to outlet is small enough to be neglected and the total temperature difference from outlet to inlet is also very small. To investigate the effect of water saturation on the temperature distribution, a single phase simulation is also performed in the PEMFCs Module in Fuent® software. Figs. 7–9 show the temperature on the cross-section of $Z = 0.05$ m (cathode inlet), $Z = 0.025$ m (middle), $Z = 0$ m (cathode outlet) for the single phase simulation. It can be seen that the relative high temperature area is in the middle cross-section which is reasonable for the counter flow pattern in PEMFCs. For demonstrating the effect of water saturation, the temperature in the same position of the present model is shown in Fig. 10 ($Z = 0.05$ m), Fig. 11 ($Z = 0.025$ m) and Fig. 12 ($Z = 0$).

First, the comparison between the cathode inlet for the two cases (present model and single phase model) are executed. It is obvious that the temperature distribution are nearly the same, which is consistent with the fact that there is nearly no liquid water due to the vaporization of the produced water and little accumulation. And it also demonstrates the correctness the present model Secondly, the temperature difference between middle cross-section is checked, and it is found that the relative high temperature area for the present two phase flow model is greatly larger than that of single phase simulation. That means the liquid water affects the heat transfer in the PEMFCs, and it hinders the heat transfer due to its relative high thermal capacity and low thermal conductivity. The same difference is also obtained for the cross-section of $Z = 0$, where the difference is more obvious for the increase of water saturation. It can be seen that the relative high temperature area is in the GDL and catalyst layer neighboring to the gas channel, but not neighboring to the current collector ribs, although where the water saturation

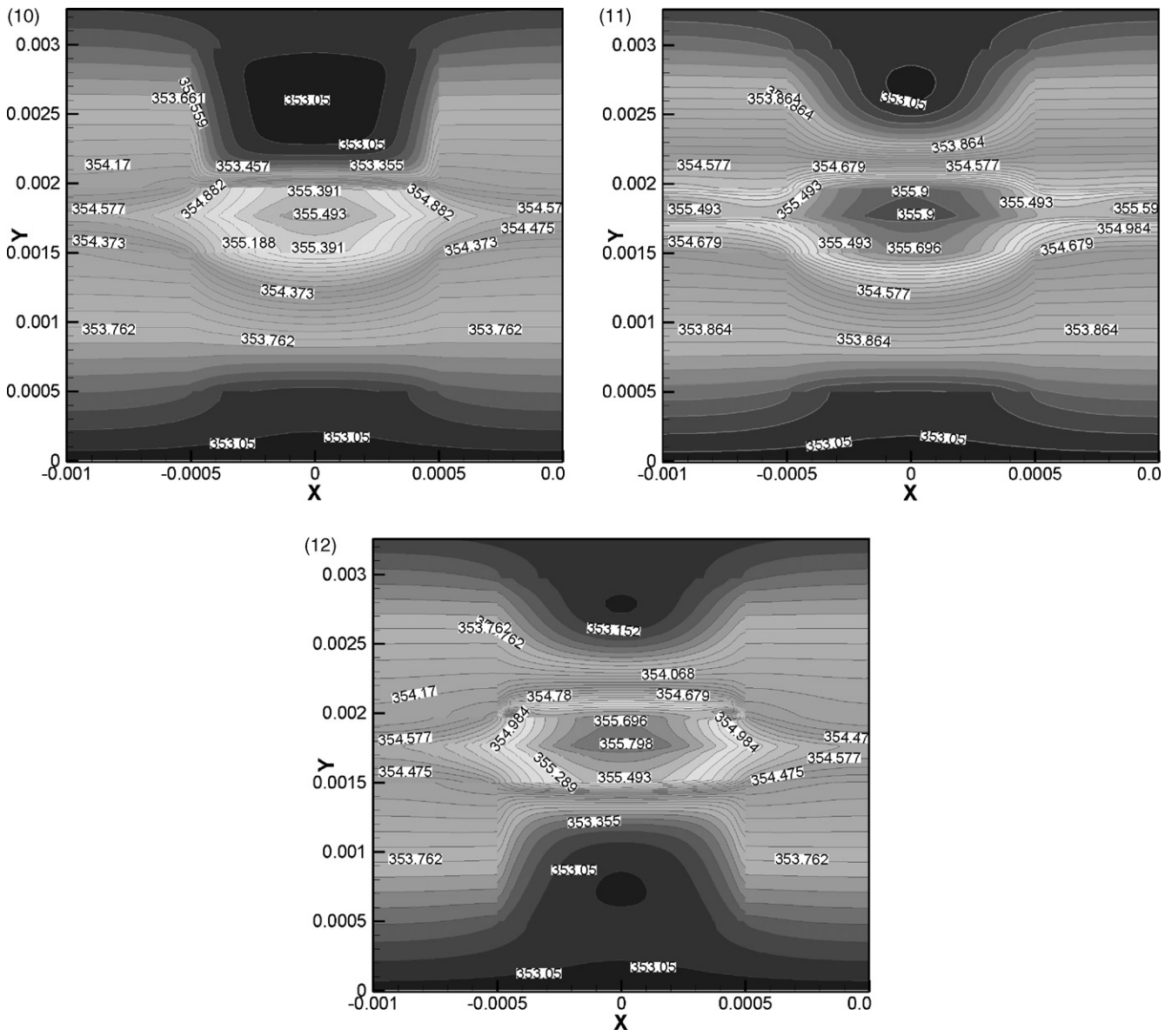

Fig. 10-Fig. 12. Temperature for the cross-section of $Z = 0.05$ m, $Z = 0.025$ m, $Z = 0$ m for the base case, *k*.

is high. This may be caused by the fact that the thermal transfer capacity of cathode gas is largely small than that of solid materials of the current collector, and also the current collector boundary is assumed to be ideally cooled So, although the water saturation is low in the area of GDL near gas channel compared with that of near current collector, it has important effect on the heat transfer, which has been shown in Fig. 12.

3.4. The effect of flow pattern on the temperature

According to the results of the present work (Fig. 10–12), It can be observed that the maximum hot area appears at the middle of the PEMFCs for the inlet of the cathode and anode are both kept at the constant temperature (353 K) in this study for counter flow pattern. To make insight into the heat transfer difference between the counter flow pattern and coflow pattern, the simulation for coflow pattern is also performed with the present model. Figs. 13–15 shows the temperature for the cross-section of $Z = 0.05$ m, $Z = 0.025$ m and $Z = 0$. And Fig. 16 shows the slices views of water saturation in the PEMFCs. It can be seen that the inlet temperature for coflow pattern is relative low than that of counter flow pattern (cathode inlet), which is due to the cooling effect of the inlet gases of both cathode side and anode side. As for the temperature distribution in the middle cross-section, it is obvious that the relative high temperature area of counter flow pattern is large than that of coflow pattern. And for the outlet cross-section, the maximum temperature is about 356.12 K for coflow pattern, which is larger than that of counter flow pattern, and consistent with the water saturation distribution in Fig. 16. So, the characters of the temperature distribution for the coflow pattern is different from the counter flow pattern, and the larger temperature difference as well as water saturation are produced, which is very important and disadvantageous for the operation of PEMFCs.

3.5. The effect of droplet size on the water saturation

In the two phase flow for the liquid droplets or solid particles in the gas phase, the size of the particles (droplets) is a key factor, which directly determine the two phase flow pattern and disperse phase (droplet or particle) behavior. It can be seen that the droplet

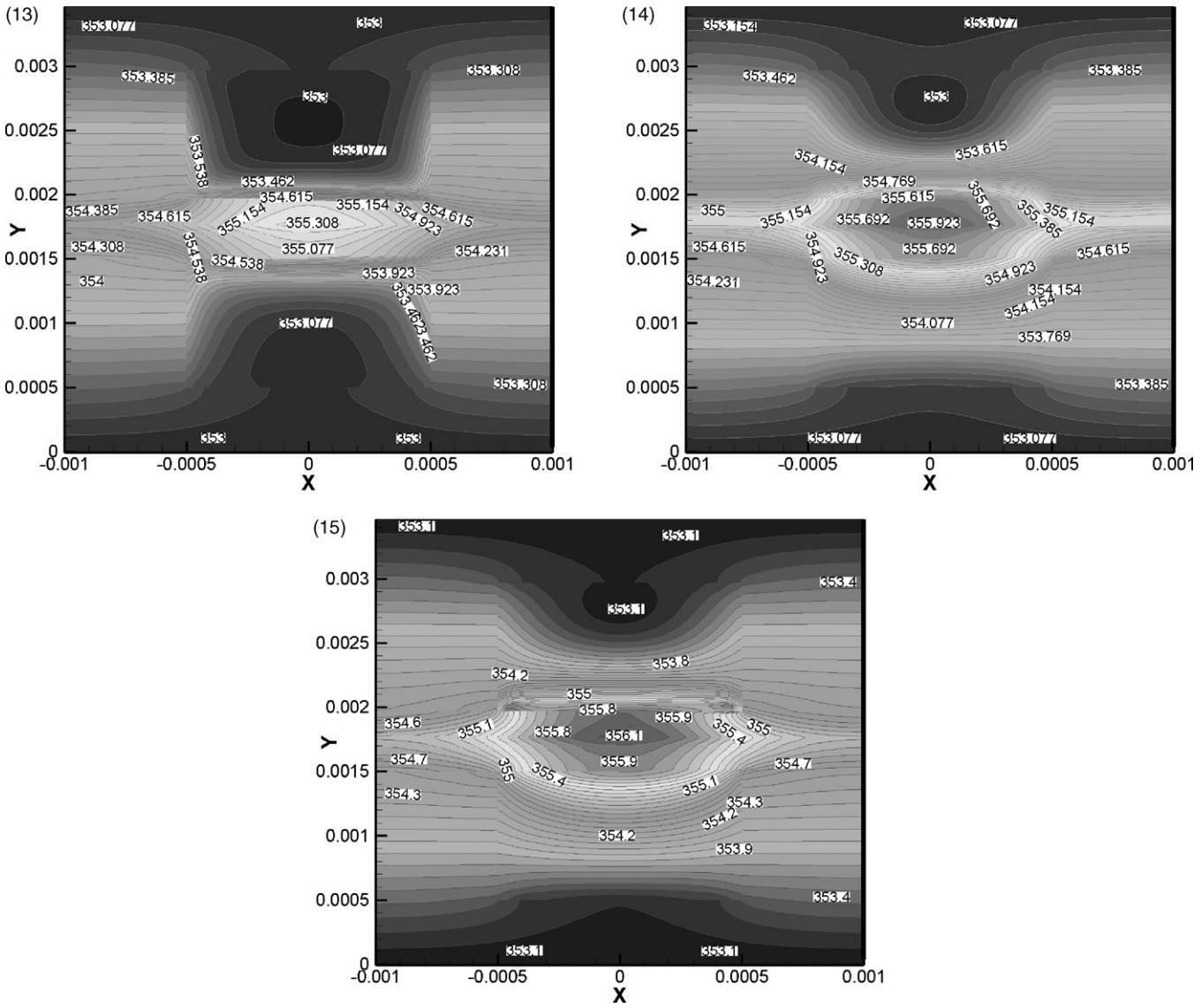

Fig. 13-Fig. 15. Temperature for the cross-section of $Z = 0.05$ m, $Z = 0.025$ m, $Z = 0$ m for the coflow pattern case, *k*.

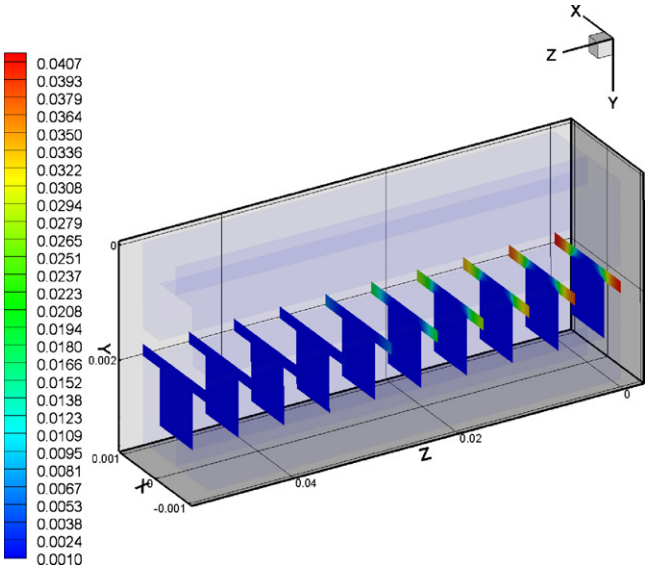

Fig. 16. Water saturation for coflow pattern.

relax time increases with the increase of the droplet size according to Eq. (11), which means the large droplet needs more time to obtain the same velocity with the small droplet, and, if the droplet is large enough, then the value of relax time is very big, that means the dominated motion of the droplet will not be flowing with the gas, so, large droplet (the ratio between the characterize size and the gas channel height above 0.5) [5] for the very low gas velocity cannot be considered in this model, the same for the other two-fluid model. And, in this case, VOF model is more suitable for the two phase simulation. Figs. 17 and 18 show (100 μm and 200 μm, the droplet size for the base case is about 145 μm) the water saturation for the different droplet size. It is obvious that the water saturation increases with the increase of droplet size, which means the large droplet is difficult to be removed and has more effect on the water saturation in GDL and catalyst layer.

However, in the PEMFCs, the effect of the gas channel properties on the liquid removal is also very important, which has been demonstrated by the experiment, so, to truly simulate the two phase behavior in PEMFCs, the parameters reflecting the gas channel properties should be considered, such as the contact angle of the gas channel wall, but all of the models for the whole PEMFCs in the reference fail to do that. In the future work, we plan to explore the

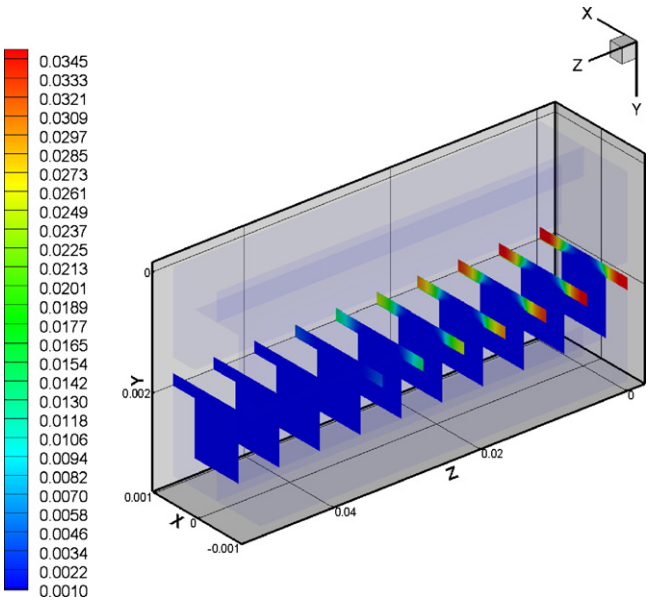

Fig. 17. Water saturation for the droplet size of 100 μm.

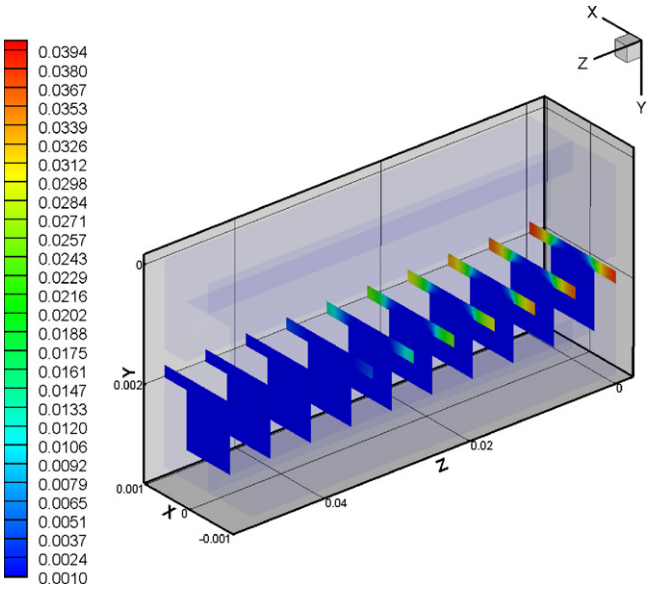

Fig. 18. Water saturation for the droplet size of 200 μm.

relationship between the gas channel contact angle and the size of water droplet (or film), and by this way, the effect of the gas channel can be included in the present model, which is more closely to the true condition of the PEMFCs.

4. Conclusions

A droplet size dependent multiphase mixture model is developed for the two phase simulation of the PEMFCs in this paper, and the droplet size in the gas channel can be considered as a parameter in this mixture model which is different from the commonly used multiphase mixture model in the reference, and the effect of gas diffusion layer (GDL) properties and the gas drag function on the liquid water removal can be integrated into the droplet size as a parameter. And it is calculation cost effective for the present model compared with the two-fluid model (which also includes the effect of the droplet size). The three-dimensional two phase simulation of the PEMFCs with a straight flow field is performed, and the heat transfer is also included. The effect of droplet size on the liquid remove, the effect of liquid water on the heat transfer and the effect of gas flow pattern on the temperature distribution are mainly investigated. The simulation results show that the large droplet is hard to be dragged by the gas, so it produces large water saturation. The results of the heat transfer show that the liquid water hinders the heat transfer in the GDL and catalyst layer, so it produces the large relative high temperature area, and the liquid water has important effect on the heat transfer in the area of GDL and catalyst layer near the channel due to the low capacity of heat transfer of the gas. The results show there is large temperature difference and water saturation in the PEMFCs operated with coflow pattern compared with counter flow pattern, which is disadvantageous for the operation of PEMFCs.

References

[1] K. Tüber, D. Pócza, C. Hebling, Journal of Power Sources 124 (2003) 403–414.
[2] A. Hakenjos, H. Muenter, U. Wittstadt, C. Hebling, Journal of Power Sources 131 (2004) 213–216.
[3] X.G. Yang, F.Y. Zhang, A.L. Lubawy, C.Y. Wang, Electrochemical and Solid-State Letters 7 (2004) A408–A411.
[4] P.K. Sinha, P. Halleck, C.-Y. Wang, Electrochemical and Solid-State Letters 9 (2006) A344–A348.
[5] F.Y. Zhang, X.G. yang, C.Y. Wang, Journal of the Electrochemical Society 153 (2006) A225–232.
[6] E. Kimball, T. Whitaker, I.G. Kevrekidis, J.B. Benziger, ECS Transactions 11 (2007) 725–736.
[7] E. Kimball, T. Whitaker, Y.G. Kevrekidis, J.B. Benziger, AIChE Journal 54 (2008) 1313–1332.
[8] H. Sun, H. Liu, L.-J. Guo, Journal of Power Sources 143 (2005) 125–135.
[9] Z.H. Wang, C.Y. Wang, K.S. Chen, Journal of Power Sources 94 (2001) 40–50.
[10] U. Pasaogullari, C.-Y. Wang, K.S. Chen, Journal of the Electrochemical Society 152 (2005) A1574–A1582.
[11] H. Meng, C.-Y. Wang, Journal of the Electrochemical Society 152 (2005) A1733–A1741.
[12] H. Masuda, K. Ito, T. Oshima, K. Sasaki, Journal of Power Sources 177 (2008) 303–313.
[13] V. Gurau, R.V. Edwards, J. Adin Mann Jr., T.A. Zawodzinski, Electrochemical and Solid-State Letters 11 (2008) B132–B135.
[14] G. He, P. Ming, Z. Zhao, A. Abudula, Yu Xiao, Journal of Power Sources 163 (2007) 864–873.
[15] K. Jain, J. Vernon Cole, S. Kumar, A. Gidwani, N. Vaidy, ECS Transactions 16 (2) (2008) 45–56.
[16] T. Berning, ECS Transactions 16 (2) (2008) 23–34.
[17] M. Manninen, V. Taivassalo, S. Kallio, On the Mixture Model for Multiphase Flow, VTT Publications, 1996.
[18] R. Clift, J.R. Grance, M.E. Weber, Bubbles, Drops and Particles, Academic press, New York, 1978.
[19] Simonin, Eulerian formulation for particle dispersion in turbulent two-phase flows, 5th Workshop on Two-phase Flow Predictions, 1990, pp. 156–166.
[20] P.K. Sinha, C.-Y. Wang, A. Su, International Journal of Hydrogen Energy 32 (2007) 886–894.
[21] T.E. Springer, T.A. Zawodzinski, S. Gottesfeld, Journal of Electrochemical Society 138 (8) (1991) 334–2342.
[22] X. Zhu, P.C. Sui, N. Djilali, Journal of Power Sources 172 (2007) 287–295.
[23] X. Zhu, P.C. Sui, N. Djilali, Journal of Power Sources 181 (2008) 101–115.
[24] A. Theodorakakos, T. Ous, M. Gavaises, J.M. Nouri, N. Nikolopoulos, H. Yanagihara, Journal of Colloid and Interface Science 300 (2006) 673–687.
[25] Y.H. Cai, J. Hu, H.P. Ma, B.L. Yi, H.M. Zhang, Journal of Power Sources 161 (2006) 843–848.